ACS APPLIED MATERIALS & INTERFACES

Research Article

www.acsami.org

Enzymatic Catalysis Combining the Breath Figures and Layer-by-Layer Techniques: Toward the Design of Microreactors

A. S. De León,[†] T. Garnier,[‡] L. Jierry,[‡,§,⊥] F. Boulmedais,[‡,§] A. Muñoz-Bonilla,*[,#] and J. Rodríguez-Hernández*[,†]

[†]Instituto de Ciencia y Tecnología de Polímeros (ICTP), Consejo Superior de Investigaciones Científicas (CSIC), C/Juan de la Cierva 3, 28006 Madrid, Spain

[‡]Institut Charles Sadron, Centre National de la Recherche Scientifique, Université de Strasbourg, UPR 22, 23 rue du Loess, BP 84047, 67034, Strasbourg Cedex 2, France

[§]Institute of Advanced Study, University of Strasbourg, 5 allée du Général Rouvillois, 67083 Strasbourg, France

[⊥]Ecole de Chimie, Polymères et Matériaux, Université de Strasbourg, 25 rue Becquerel, 67087 Strasbourg, France

[#]Departamento de Química-Física Aplicada, Facultad de Ciencias, Universidad Autónoma de Madrid, C/Francisco Tomás y Valiente 7, Cantoblanco, 28049 Madrid, Spain

Supporting Information

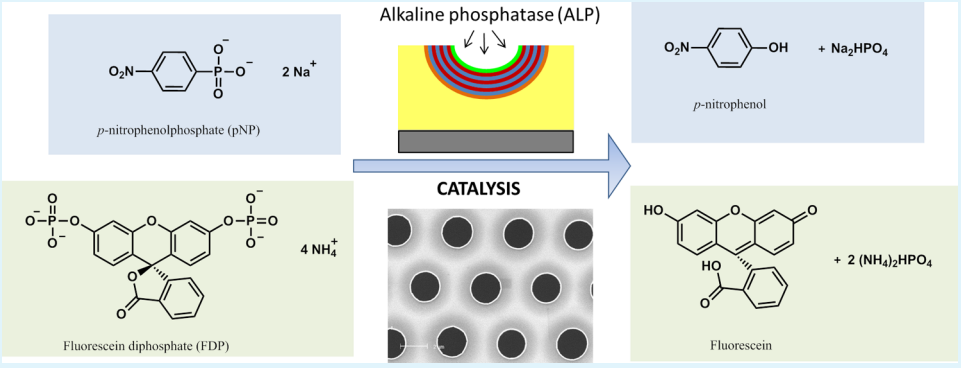

ABSTRACT: Herein, we report the fabrication of microstructured porous surfaces with controlled enzymatic activity by combining the breath figures and the layer-by-layer techniques. Two different types of porous surfaces were designed based on fluorinated and carboxylated copolymers in combination with PS, using poly(2,3,4,5,6-pentafluorostyrene)-*b*-polystyrene ($PS5F_{31}$-*b*-PS_{21}) and polystyrene-*b*-poly(acrylic acid) (PS_{19}-*b*-PAA_{10}) block copolymers, respectively. For comparative purposes, flat surfaces having similar chemistry were obtained by spin-coating. Poly(sodium 4-styrenesulfonate)/poly(allylamine hydrochloride) (PSS/PAH) multilayers incorporating alkaline phosphatase (ALP) were built on these porous surfaces to localize the enzyme both inside and outside of the pores using PS/$PS5F_{31}$-*b*-PS_{21} surfaces and only inside the pores on PS/PS_{19}-*b*-PAA_{10} surfaces. A higher catalytic activity of ALP (about three times) was obtained with porous surfaces compared to the flat ones. The catalysis happens specifically inside the holes of PS/PS_{19}-*b*-PAA_{10}surfaces, where ALP is located. This opens the route for applications in microreactors.

KEYWORDS: *breath figures, multilayers, polyelectrolytes, surface modification, catalysis of porous supports, enzymatic catalysis, alkaline phosphatase, surface-confinement, microreactor design*

INTRODUCTION

The design of materials for heterogeneous catalysis has been of great interest during the last years. In comparison with homogeneous catalysis, the wide applicability combined with the easy possibility of recycling the catalyst make these new materials very attractive.[1] Many different supported catalysts have been described in the literature. For instance, metals supported on carbon nanotubes,[2−4] graphene-based materials,[5] hollow nanoparticles,[6] inorganic nanoparticles embedded in hydrogels,[7] photocatalysts to produce fuels,[8] etc. In addition, the immobilization of enzymes has been reported in view of their use as biocatalysts.[9]

Within this area, the field of micro- and nanoreactors, which consists in the fabrication of materials with defined patterned areas containing compounds with catalytic activity, is getting more and more attention.[10] Microreactors have allowed for integrating the exact conditions of a conventional reactor in the

Received: March 25, 2015
Accepted: May 18, 2015
Published: May 18, 2015

DOI: 10.1021/acsami.5b02607
ACS Appl. Mater. Interfaces 2015, 7, 12210−12219

macroscale but in a reduced volume. Advantages include less consumption of material, improved contact between the diverse reactants and increased control of heat and mass transfer, which leads to an increase of the conversion. Also, these materials have potential applications as miniature high-throughput screening templates.[11] Microfluidics is, by far, the most widely used technique.[12−14] However, other techniques to create micropatterned surfaces, such as lithography,[15,16] etching[17] or sol−gel procedures[18] are also under investigation.

In this sense, the breath figures technique is an interesting alternative. This inexpensive, easy, and fast technique permits the design of polymeric templates with a tunable and controlled pore size, typically ranging from 100 nm to 20 μm. The formation of breath figures occurs when a polymeric solution in a volatile solvent is drop cast inside a closed chamber with high relative humidity. During the evaporation of the solvent, the solvent/air interface is cooled and micrometric droplets of water condense on the surface. Finally, the evaporation of the condensed water leads to a porous film that may, in some cases, produce regular patterned honeycomb porous films. The use of breath figures as catalytic supports have some interesting advantages. First, porous materials exhibit a larger surface area when compared to a flat surface. Besides, the functionality of the surface can be precisely controlled inside, outside or both inside and outside of the pores. For instance, when a hydrophilic copolymer is employed as additive in polymer blends, the hydrophilic groups direct this additive toward the interface with the water droplets, remaining there after the film is formed.[19,20] As a result, the pore composition can differ to a large extent to the rest of the surface. This has potential application in the design of microreactors, as the pores will be selectively enriched in a determined compound that could catalyze a specific reaction. In this paper, we describe the preparation of porous materials with catalytic activity over the entire surface and porous surfaces with active sites localized inside of the pores. In the latter, because the pores are micrometer-sized, they can be considered as microreactors.

There are several publications evidencing the potential of surfaces formed by breath figures in catalysis.[21,22] Most of the reports considered the possibility of decorating the pores with inorganic nanoparticles which is also of great interest for catalytic applications.[23] For instance, recently, Naboka et al. have fabricated a honeycomb-patterned surfaces containing a cobalt salt in "one pot" system, although it was not reported promising uses in catalysis.[24] Dong et al. deposited silver nanoparticles with catalytic activity in the reduction of organic dyes.[25] Recently, Pessoni et al.[26] reported the design of porous films containing a photocatalyst. These films were able to produce singlet oxygen, with an activity five times higher when compared to a flat surface with the same composition.

In this manuscript, we will focus on the surface immobilization of enzymes testing their catalysis. In particular, alkaline phosphatase (ALP) is an enzyme of great interest due to its role in the mechanism of new bone formation, splitting off inorganic phosphates from organic substrates.[27] To the best of our knowledge, only one example has been reported concerning the immobilization of enzymes onto honeycomb films. Wan et al.[28] fabricated porous films containing enzyme horseradish peroxidase nanoparticles composed of an enzyme core and a cross-linked polymer shell. However, their catalytic assays were limited to proof the stability of the nanoparticles versus the free enzyme on porous films.

The layer-by-layer method consists on the formation of nanoassembled thin films by alternated deposition of oppositely charged polyelectrolytes.[29,30] Spherical particles or hollow capsules[31,32] can also easily be formed when the buildup is performed on the surface of preformed particles. Multilayer films obtained by hydrogen bonding,[33] click chemistry,[34] hydrophobic,[35] or host−guest interactions[36] are also widely reported. Raising a special interest in this technology in the biomedical field,[37] these films have potential applications in the encapsulation and/or immobilization of proteins and enzymes. A wide variety of enzymes including catalase, peroxidase, urease, or glucose oxidase have been embedded using multilayer deposition.[38]

In this work, we propose the use of breath figures with controlled surface chemistry by using multilayers of polyelectrolytes as supports to immobilize an enzyme (i.e., ALP). The control over the chemistry of the porous surface will allow us to prepare multilayers inside and outside the pores or exclusively inside the pores. Their fabrication and the evaluation of the catalytic properties of the films will be described in detail.

EXPERIMENTAL SECTION

Materials. Polyethylenimine (PEI, branched, M_w = 25,000 g/mol), poly(sodium 4-styrenesulfonate) (PSS, M_w = 70,000 g/mol), poly(allylamine hydrochloride) (PAH, M_w = 58,000 g/mol) and high molecular weight polystyrene (PS, M_w =2.50 × 10^5 g/mol) were purchased from Aldrich. Alkaline phosphatase (ALP) was purchased from TCI. Trizma (base, minimum 99.9% titration) was purchased from Sigma. *p*-nitrophenyl phosphate (pNP, disodium salt hexahydrate, 98%) was purchased from Alfa-Aesar. Fluorescein diphosphate (FDP, tetraamonium salt) was purchased from Life Technologies. Triethylamine (TEA), dichloromethane (DCM), chloroform, carbon sulfide (CS_2) and dimethyl sulfoxide (DMSO) were purchased from Scharlau. All products were used as received. All solutions were prepared using ultrapure water (Milli Q-plus system, Millipore, Molsheim, France) with a resistivity of 18.2 MΩ cm.

Preparation of the Block Copolymers and Fabrication of Honeycomb-Patterned Films by the Breath Figures Technique. Polystyrene-*b*-poly(acrylic acid) (PS_{19}-*b*-PAA_{10}) was synthesized via Atom transfer radical polymerization (ATRP) according to previously reported procedures.[39] Briefly, first a PS macroinitiator was synthesized by ATRP, and subsequently, a *tert*-butyl acrylate was polymerized. Finally, the acrylic acid groups were obtained by adding trifluoroacetic acid (excess) in dichloromethane thus removing the *tert*-butyl groups. Poly(2,3,4,5,6-pentafluorostyrene)-*b*-polystyrene ($PS5F_{31}$-*b*-PS_{21}) was synthesized from a $PS5F_{31}$ macroinitiator also made by ATRP ($PS5F_{31}$−Br).[40]

Synthesis of Thiolated Branched Polyethylenimine (PEI-SH). Branched poly(ethylene imine) (1.0 g, 33 mmol of ethylene imine groups) was dissolved in 40 mL of dried dichloromethane. Then, N-succidimidyl-3-mercaptopropionate (0.945 g, 4.65 mmol) (prepared according to[41]) was added and the reaction mixture was stirred for 24 h at room temperature. A yellowish slurry mixture was obtained. Organic solvent was removed under reduced pressure and the residue was dissolved in water. Dialysis of this aqueous solution against five liters of deionized water during 5 days (cutoff membrane: 2 kDa) and freeze-dried of the solution lead to 1.9 g of colorless solid. ^{1}H NMR (D_2O, 400 MHz): δ(ppm) 2.60−3.20 (broad m, 4H, NH−C$\underline{H_2}$−C$\underline{H_2}$), 3.35 (broad s, 2H, C$\underline{H_2}$−CH_2−SH), 3.55 (broad s, 2H, CH_2−C$\underline{H_2}$-SH). Comparison of the integration of the signal at 3.55 ppm and the integration of the mass if between 2.60 and 3.20 ppm leads to a modification degree of 10%.

Film Fabrication. In a typical procedure, porous films were prepared by drop casting a mixture of high molecular weight PS used as matrix and the block copolymer in a chloroform or carbon disulfide solution under saturated relative humidity (98%) conditions at room

DOI: 10.1021/acsami.5b02607
ACS Appl. Mater. Interfaces 2015, 7, 12210−12219

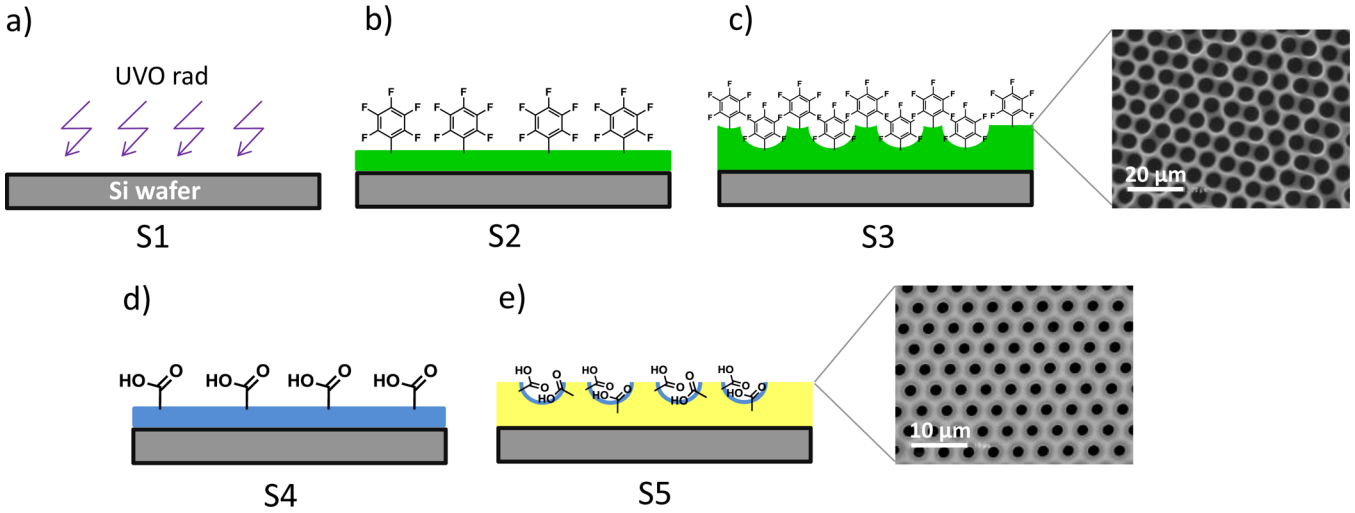

Figure 1. Scheme depicting the different surfaces used in this publication; (a) silicon wafer irradiated with UV light (S1); (b) blend containing PS and $PS5F_{21}$-*b*-PS_{31} spin coated (S2); (c) blend containing PS and $PS5F_{21}$-*b*-PS_{31} casted under high relative humidity conditions (S3); (d) blend containing PS and PS_{19}-*b*-PAA_{10} spin coated (S4); (e) blend containing PS and PS_{19}-*b*-PAA_{10} casted under high relative humidity conditions (S5). SEM micrographs of S3 and S5 are also shown.

temperature inside a closed chamber. In the case of PS_{19}-*b*-PAA_{10}, carboxylic acid groups are expected to be preferentially located inside the pores, while when using $PS5F_{31}$-*b*-PS_{21} fluorinated groups are expected to be homogeneously distributed along the whole surface.[39,40] For the preparation of the surfaces, 20 mg/mL polymer concentrations were employed. The amount of copolymer within the blend was varied between 20 and 50 wt %.

For comparative purposes, flat surfaces were also prepared. First, silicon wafers of 1 cm^2 approximately were cleaned with water and ethanol. Then, the same solutions used in the preparation of the porous surfaces (depicted above) were spin coated at 2000 rpm in order to obtain flat surfaces that could be compared with the porous ones. Also, bare silicon wafers were used. In this case, these surfaces were exposed to a UVO treatment for 3 min prior to their use. A scheme containing all the surfaces that will be used is shown in Figure 1.

Layer-by-Layer Buildup. Multilayer films were built with a rotatory multistep coater (Nadetech Innovations, Spain) on the previously described surfaces. Flat surfaces were dipped into the polyelectrolyte solutions with a concentration of 0.5 mg/mL (150 mM NaCl) for 5 min. Then, they were rinsed in a 150 mM NaCl solution for 5 min. In the case of the porous surfaces, the dipping time was increased up to 45 min to be sure that the solution is able to fill the holes. First, a PEI layer was placed on all the different surfaces. In the case of the fluorinated surfaces (S2, S3), a thiol-modified PEI was used in a mixture 1:1 of Milli-Q:DMSO with an excess of TEA to be sure that covalent interaction via click chemistry happens. Then, subsequent layers of PSS/PAH were adsorbed by dipping. After deposition of *n* bilayers, the film is denoted $(PSS/PAH)_n$. The enzyme alkaline phosphatase (ALP) was deposited on $(PSS/PAH)_n$ film. Typically, 3 bilayers of PSS/PAH and a final layer of ALP (or fluorescently labeled ALP^{RhoB} for fluorescence experiments[42]) were deposited on the different surfaces. In the case of ALP, the dipping time for the flat surfaces was increased to 10 min, whereas that for the porous was maintained at 45 min. The rinsing time was of 5 min in all cases. All surfaces were rapidly dried after the buildup to avoid salt crystallization.

Characterization of the Surfaces. Measurement of the film thickness was carried out with a PLASMOS SD 2100 instrument operating at the single wavelength of 632.8 nm and at constant angle of 45°.The refractive index of all polyelectrolyte films was assumed to be constant at $n = 1.465$. For each surface studied, at least 10 points were measured to obtain the average value for the film thickness and to determine the film homogeneity. Water contact angles (CA) were measured using a KSV Theta goniometer. The volume of the droplets was controlled to be about 2.0 μL and a charge coupled device camera was used to capture the images of the water droplets for the determination of the contact angles. Fluorescence microscopy was performed using an Eclipse Ti−S of Nikon fluorescence microscope with a DS-Qi 1Mc coupled camera device. Images were acquired using the set filters for red fluorescence (λ_{ex} = 542−582 nm, λ_{em} = 604−644 nm).

Measurement of the Catalytic Activity. The alkaline phosphatase activity was detected using two different enzymatic substrate molecules: *p*-nitrophenyl phosphate (pNP) and fluorescein diphosphate (FDP). In the case of pNP (colorless), 2 mL of a solution of pNP (10 mM) in 150 mM NaCl/10 mM Tris buffer (pH 8.0) were placed into a 6 wells Costar microplate containing the surface to study. A multidetector spectrofluorimeter (Xenius XC, SAFAS, Monaco) equipped with a microplate reader was used to monitor the absorbance of *p*-nitrophenol (yellow) in the supernatant, which mirrors the catalytic activity of enzymes within the surface. Absorbance of *p*-nitrophenol was monitored at a wavelength of 405 nm every 90 s for 2 h. An additional experiment to test the catalytic activity of the enzyme was carried out up to 2 days. All experiments were repeated at least 3 times to be sure that the results are reproducible. For the experiments performed with FDP, a droplet of 0.1 mL of the solution (0.1 mg/mL FDP in 150 mM NaCl) was placed on top of the surface and fluorescence intensity of fluorescein (product of the enzyme) was measured every 10 min with an Eclipse Ti−S of Nikon fluorescence microscope with a DS-Qi 1Mc coupled camera device. Images were acquired using different magnifications (10× and 40×) and the set filters for green fluorescence (λ_{ex} = 457−487 nm, λ_{em} = 502−537 nm) and red fluorescence (λ_{ex} = 542−582 nm, λ_{em} = 604−644 nm). The analysis of fluorescence intensity was performed using the image analysis software (ImageJ, http://rsb.info.nih.gov/ij/).

RESULTS AND DISCUSSION

Formation of the Planar/Porous Supports. Fresh silicon wafers were cleaned in a UVO chamber for 3 min to remove dusts and produce a hydrophilic and negatively charged layer of silicon oxide (Figure 1). The obtained surface, named S1, will be used to optimize the conditions for the growth of a first layer of positively charged PEI and subsequently multilayer formation. Surfaces S2 and S3, respectively flat and porous, were prepared from the same mixture of $PS5F_{31}$-*b*-PS_{21} (50 wt %) and PS in CS_2. Surfaces S4 and S5, respectively flat and porous, were prepared from a mixture of PS_{19}-*b*-PAA_{10} (20 wt

DOI: 10.1021/acsami.5b02607
ACS Appl. Mater. Interfaces 2015, 7, 12210−12219

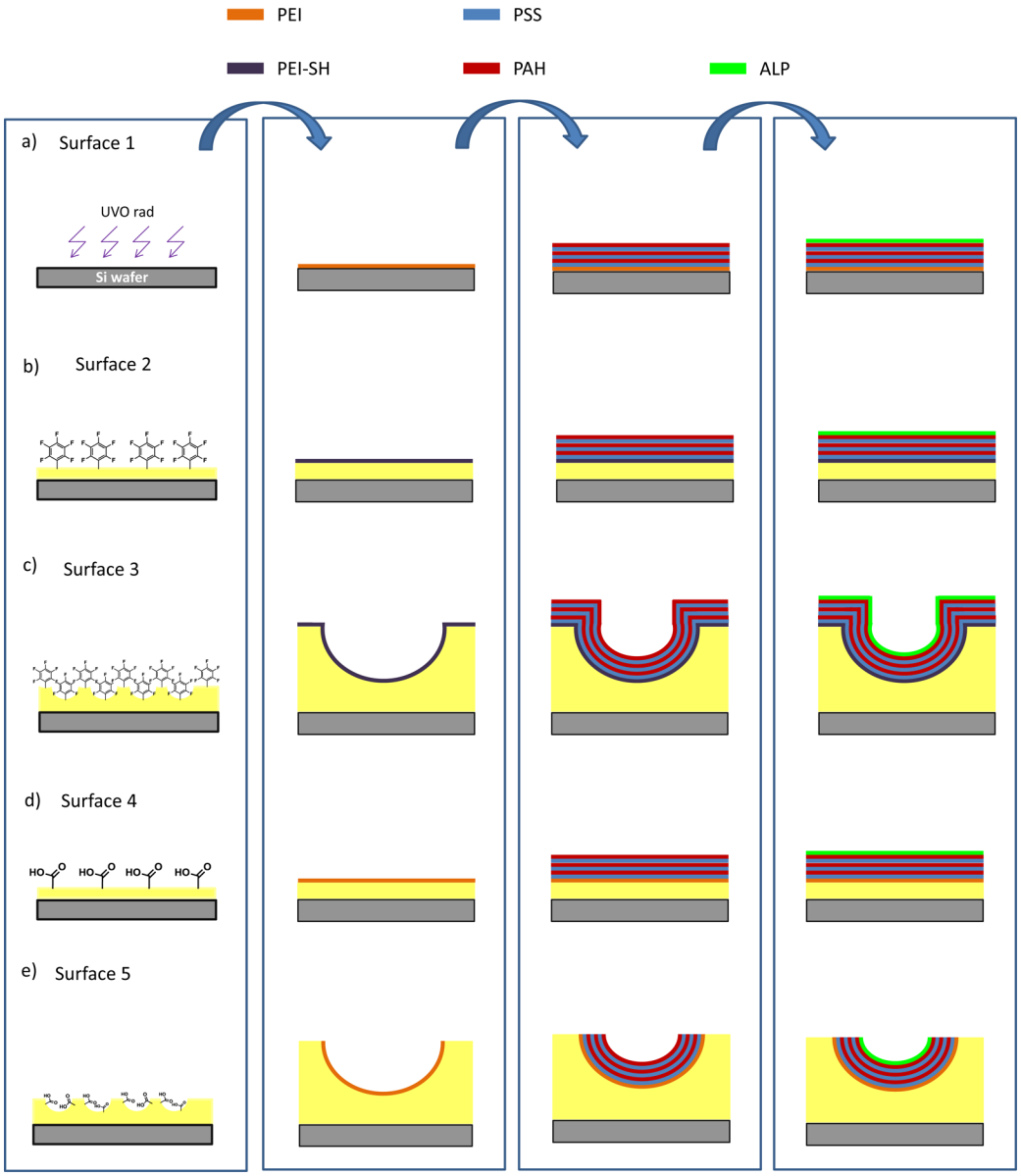

Figure 2. Strategy followed to prepare layer-by-layer films on either planar or porous surfaces followed by the immobilization of alkaline phosphatase (ALP). Surface S1: UVO cleaned silicon wafer. Surface S2: planar surface prepared by spin coating of a blend (50/50) wt % of polystyrene and the block copolymer $PS5F_{31}$-*b*-PS_{21}. Surface S3: porous films obtained by the breath figures approach having 50 wt % of $PS5F_{31}$-*b*-PS_{21} and 50 wt % of polystyrene. Surface S4: planar surface prepared by spin coating of a blend (80/20) wt % of polystyrene and the block copolymer PS_{19}-*b*-PAA_{10}. Surface S5: porous films obtained by the breath figures approach having 20 wt % of PS_{19}-*b*-PAA_{10} and 80 wt % of polystyrene.

%) and PS in chloroform. In all cases, the total polymer concentration comprising polymer matrix (PS) and additive was set to 20 mg/mL. Porous surfaces (S3, S5) have been prepared by the breath figures method in which the solutions were injected inside a closed chamber with saturated relative humidity at room temperature onto glass coverslips. As a result, micropatterned porous surfaces with controlled topography and composition were obtained. In addition, the chemical distribution of the additives is directly related to the hydrophilicity/hydrophobicity of the functional monomers included in the additive. Upon deposition of the polymer solution onto a surface, evaporation of the volatile solvent occurs and the temperature of the solution surface decreases sharply. When the relative humidity is high enough (above 50%), small water droplets tend to condense, forming a porous pattern when the film is completely dried. More interestingly, when using an amphiphilic additive (e.g., PS_{19}-*b*-PAA_{10}, S5), the hydrophilic groups tend to migrate toward the interface with the condensed water droplets stabilizing them. As a result, these PAA groups are preferentially located inside the pores of the surface.[39] As will be depicted later, these carboxylic acid groups will be used to interact electrostatically with a first layer of branched PEI, which will be the beginning of the layer-by-layer buildup that will occur exclusively inside of the pores. When using a double hydrophobic additive ($PS5F_{31}$-*b*-PS_{21}, S3), the additive appears homogeneously distributed over the entire surface.[40] These surfaces will serve to prepare multilayered films homogeneously distributed at the porous surface. Figure 1 includes illustrative SEM images of the porous surfaces obtained either using PS_{19}-*b*-PAA_{10} or $PS5F_{31}$-*b*-PS_{21} as additives. They both produced well-ordered honeycomb porous

DOI: 10.1021/acsami.5b02607
ACS Appl. Mater. Interfaces 2015, 7, 12210−12219

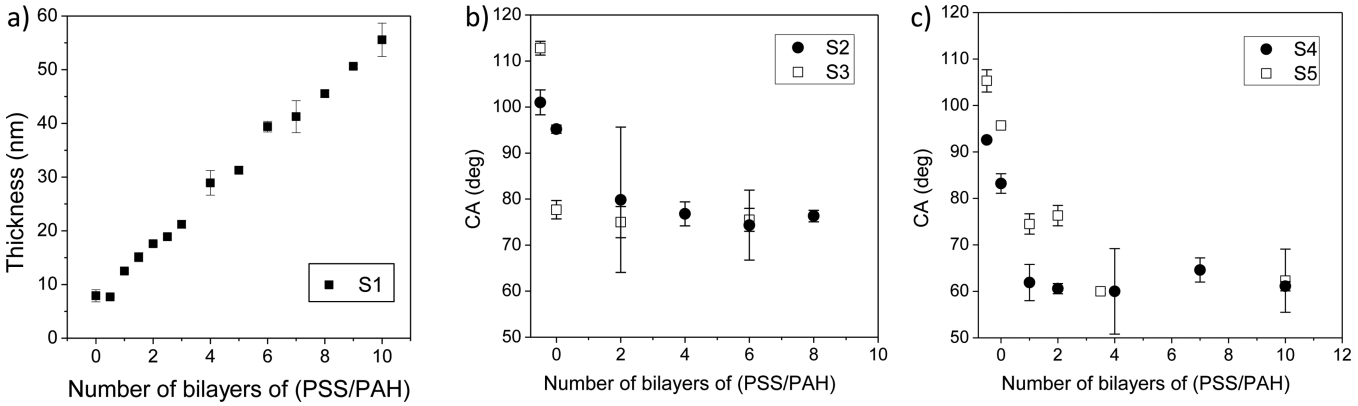

Figure 3. Buildup of PEI-$(PSS/PAH)_n$ multilayer films; (a) evolution of the thickness, measured by ellipsometry, when the film is built on silicon wafer surface S1; (b) evolution of the contact angle when the film is built on $PS/PS5F_{31}$-*b*-PS_{21} flat S2 and porous S3 surfaces and (c) on PS/PS_{19}-*b*-PAA_{10} flat S4 and porous S5 surfaces as a function of the number of PSS/PAH bilayers. Values at $x = -0.5$ and $x = 0$ in CA measurements correspond to unmodified surfaces S2−S5 and modified with PEI or PEI-SH first layer, respectively.

films with average pore diameters of 2 and 5 μm for the block copolymers PS_{19}-*b*-PAA_{10} and $PS5F_{31}$-*b*-PS_{21}, respectively.

Flat surfaces (S2, S4) have been equally prepared from the blends for comparative purposes. In this case, the solutions were spin-coated at 2000 rpm onto a silicon wafer in a chamber with low humidity to avoid water condensation.

Construction of the Multilayered Films onto the Porous/Planar Films. The strategy employed to prepare the multilayered structures is depicted in Figure 2. Solutions of PEI, PSS, and PAH were prepared with a polymer concentration of 0.5 mg/mL in a buffer solution of 150 mM NaCl. In all cases, pH was set to 5−6 in the cases of PSS and PAH, and ∼9 for PEI. The adjustment of the pH is particularly important in the case of the surfaces containing acid groups (S4, S5), because at pH 9 we ensure both that the carboxylic groups are deprotonated and that the electrostatic interactions with the first layer of branched PEI will occur.[43]

The formation of the multilayers requires an initial PEI layer. For surfaces S1, S4, and S5, a first layer of PEI was obtained by simple dipping since the carboxylic groups present at the interface will serve to anchor PEI by electrostatic interactions. In the case of fluorinated surfaces S2 and S3, an alternative way was applied to coat the surface with PEI. Indeed, PEI does not adsorb strongly enough onto fluorinated surface. Thus, we modified the PEI with thiol groups to get branched PEI-SH. When PEI-SH solution is brought in contact with fluorinated surfaces, an aromatic substitution of the fluorine atom in *para* position of the pentafluorophenyl group by the free thiol occurs. This fast and efficient transformation is considered as a click reaction and leads to an irreversible covalent bond.[40] Thus, a PEI-SH solution at 0.5 mg/mL in a DMSO:H_2O 1:1 solution in the presence of TEA was used to covalently anchored the first PEI layer.

Afterward, the PEI-functionalized surfaces allowed building the multilayers by alternated deposition of PSS and PAH by dipping process. In the case of flat surfaces (i.e., S1, S2, and S4), the dipping time was adjusted to 5 min. The construction of the multilayers on the porous surfaces (S3, S5) was carried out using longer dipping times of 45 min for each layer. By using these conditions, we assured that the polyelectrolytes have enough time to reach the holes of the surfaces and establish the electrostatic interactions. In all cases after dipping in each polyelectrolyte solution, a rinsing step was performed in aqueous 150 mM NaCl for 5 min.

The buildup of the layer-by layer-films was followed both by ellipsometry in the case of S1 and by contact angle (CA) in the cases of S2−S5, as it can be observed in Figure 3. (PSS/PAH) system follows a linear growth (Figure 3a), which is in good agreement with previous studies.[30,44,45] Upon 10 bilayers of (PSS/PAH), an average thickness of 50−60 nm is obtained in the dry state. It was not possible to follow the growth of the film by ellipsometry in the case of surfaces S2−S5 because of either PSS/PAH film thickness, which is negligible in comparison with the total film thickness or the porous morphology of surfaces. As an alternative, CA measurements provide qualitative results that permit to follow the multilayer construction. Before the deposition of the first layer, a higher contact angle is appreciated in the porous surfaces (S3, S5) than their respective flat surfaces (S2, S4). This is caused by the hydrophobicity of the material (PS mostly) and the roughness of the surface, and can be explained by the Cassie−Baxter state.[40] After the deposition of a polyelectrolyte layer, the hydrophobicity of the surface decreases, provoking a decrease of the contact angle. In the case of the fluorinated surfaces (S2, S3), it has been observed a sharp decrease of the contact angle upon the construction of the first two layers. Then, the contact angle remains constant with values around 70−80° (Figure 3b). In the case of the surfaces containing carboxylic acid groups (S4, S5), a similar trend can be observed (Figure 3c) reaching a limit angle around 60°. Interestingly in both cases after 4 (PSS/PAH) bilayers, practically the same values of contact angle are obtained. This can be explained by a transition from the Cassie−Baxter to the Wenzel regimes. As polyelectrolyte layers are being added, this effect disappears gradually reaching a limit defined by the Wenzel state, predicting that contact angle values are practically the same for flat and rough surfaces, which is characteristic of hydrophilic surfaces. These results are in a good agreement with those previously reported by Ke et al.[46]

Enzyme Immobilization. Once we have demonstrated that the multilayer buildup can be performed onto these polymeric surfaces, we immobilized by dipping a layer of a negatively charged enzyme, i.e. alkaline phosphatase (ALP). More precisely after 3 bilayers of PSS/PAH, flat surfaces were immersed in a solution of 0.5 mg/mL of ALP in 150 mM NaCl for 10 min, then rinsed in a 150 mM NaCl solution for 5 min. Dipping time was increased up to 10 min to ensure the complete (i.e., equilibrium state) immobilization of ALP. Longer dipping times did not produce additional changes.

DOI: 10.1021/acsami.5b02607
ACS Appl. Mater. Interfaces 2015, 7, 12210−12219

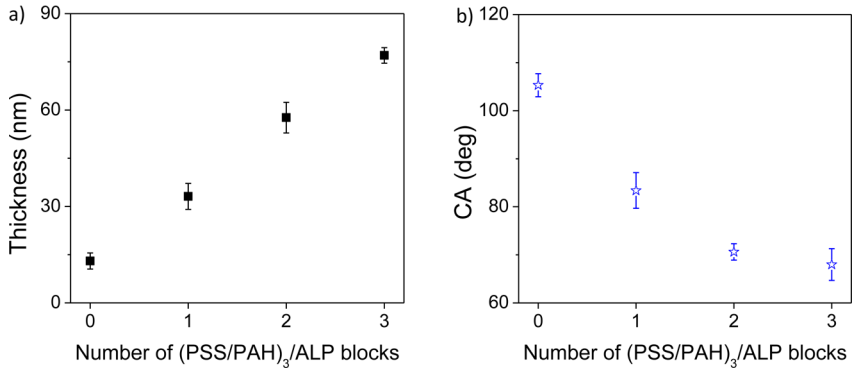

Figure 4. Buildup of $((PSS/PAH)_3/ALP)_n$ multilayer films. (a) Evolution of the thickness, measured by ellipsometry, when the film is built on surface S1 as a function of the number of layers of $((PSS/PAH)_3/ALP)$ blocks; (b) evolution of the contact angle when the film is built on PS/PS_{19}-*b*-PAA_{10} porous surface S5 as a function of the number of layers of $((PSS/PAH)_3/ALP)$ blocks.

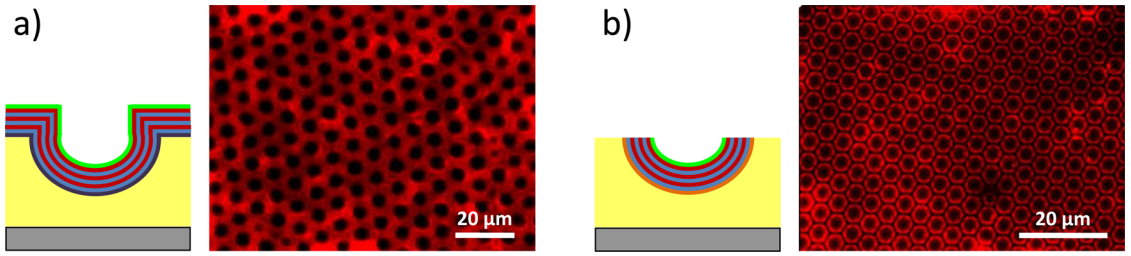

Figure 5. Fluorescence microscopy images of $(PSS/PAH)_3/ALP^{RhoB}$ multilayer films deposited on (a) fluorinated surface S3; (b) carboxylated surface S5.

For the porous surfaces S3 and S5, dipping and rinsing times were maintained at 45 and 5 min, respectively. In addition, to provide a larger amount of catalytic centers within the multilayered material, the number of deposited layers of ALP was varied. We prepared up to three repeating blocks of $(PSS/PAH)_3/ALP$ on surfaces S1 and S5 (Figure 4). The linear growth of the thickness on surface S1 can be easily appreciated, which confirms the formation of the three $(PSS/PAH)_3/ALP$ blocks (Figure 4a). Figure 4b illustrates the CA values obtained for surface S5. We can observe a fast decrease in the contact angle during the initial layers that stabilizes in the following deposition steps. This tendency is, thus, similar to the one previously obtained for PSS/PAH system shown in Figure 3c. However, in this case, the static contact angles are slightly higher. This could be caused by ALP, which is more hydrophobic than polyelectrolytes, thus making the whole system slightly less hydrophilic. Ke et al. observed this effect during the buildup of alginate/chitosan (ALG/CHI) multilayers. In this case, whenever a layer of CHI was deposited, a slight increase in the CA was observed. Then, when another layer of ALG was adsorbed, the CA decreased to a lower value.[46] This effect is explained by a higher hydrophobicity of CHI compared to ALG.

In addition, the multilayer formation and thus incorporation of ALP was evaluated by fluorescence microscopy. Previous studies, with fluorescently labeled polyelectrolytes[45,47] and with ALP,[48] show that the multilayers formed are quite homogeneous and with a constant thickness. However, up to the best of our knowledge, no similar studies have been performed with porous surfaces. Therefore, fluorescence studies were carried out on the porous surfaces $PS/PS5F_{31}$-*b*-PS_{21} (S3) and PS/PS_{19}-*b*-PAA_{10} (S5) to check the immobilization of ALP and in particular to obtain information about the distribution of ALP over the porous surfaces. A mixture of ALP (0.4 mg/mL) and ALP labeled with rhodamine B (ALP^{RhoB}, 0.1 mg/mL) in a 150 mM NaCl aqueous solution was used for this purpose. Figure 5 shows the fluorescence images that evidence a particular surface distribution of ALP^{RhoB} on the different porous surfaces. In the case of fluorinated surface S3 (Figure 5a), a homogeneous distribution of the enzyme is obtained because of the homogeneous distribution of fluorinated groups along the surface both inside and outside the pores, as previously reported.[40] In the case of carboxylated surface S5 (Figure 5b), a characteristic ring pattern is obtained. This pattern has been previously observed by our group[39] and others[49] as a proof that the fluorescent compound (i.e., ALP^{RhoB}) is specifically located only inside of the pores. This would also mean that all the previous layers deposited (branched PEI, PSS and PAH) have been also deposited inside the pores, proving that multilayers can be built selectively in a specific area of porous surfaces.

We can conclude that we were able to obtain two different distributions of the catalytic moieties in the porous surfaces, depending on the surface composition, using the same multilayer buildup strategy. On the one hand, ALP functionalized porous surfaces with higher specific surface area were obtained compared to a completely flat surface with the same chemical composition (fluorinated surfaces S3 and S4). On the other hand, we succeed in a specific immobilization of enzymes located only inside the pores (carboxylated surface S5). A more in detail study of the specific surface areas is shown in the Supporting Information. We can expect that the catalytic reaction will occur exclusively within the holes and we could use these surfaces as microtemplates or microreactors.

Study of the Catalytic Activity. ALP is an hydrolase enzyme able to remove phosphate groups on different kind of organic compounds.[27] In our study, we will use this enzyme as model and monitor its dephosphorylating catalytic activity by using two chromogenic and fluorogenic substrates: *p*-nitro-

DOI: 10.1021/acsami.5b02607
ACS Appl. Mater. Interfaces 2015, 7, 12210−12219

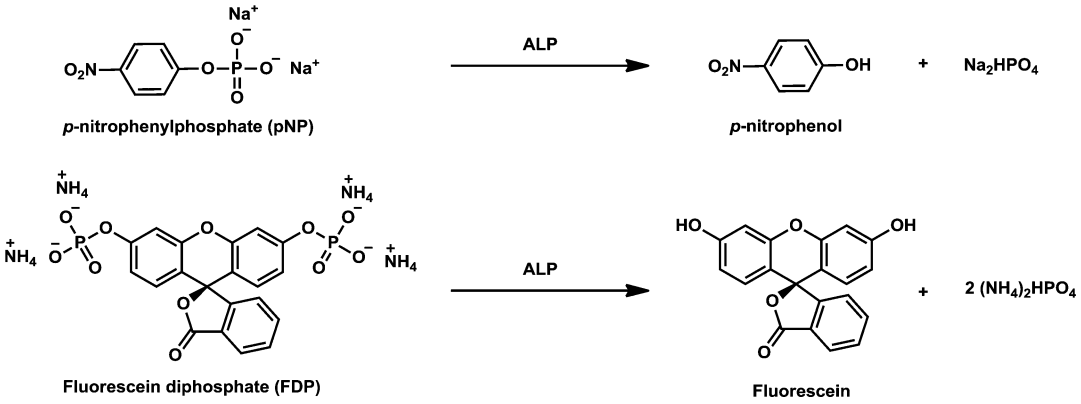

Figure 6. Scheme of the catalytic dephosphorylation of *p*-nitrophenylphosphate (pNP) and fluorescein diphosphate (FDP) in the presence of alkaline phosphatase (ALP).

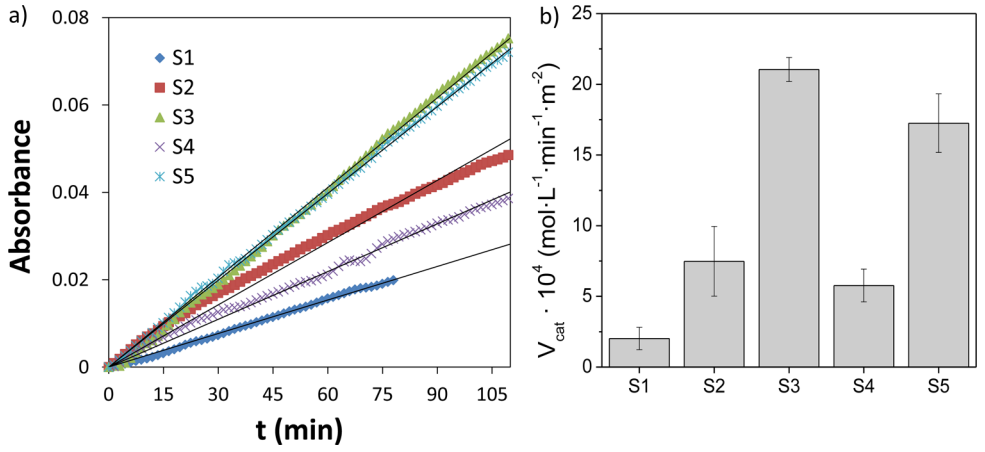

Figure 7. Catalytic activity of immobilized ALP on different surfaces; (a) evolution of the absorbance, measured at 405 nm, as a function of time corresponding to *p*-nitrophenol released by contact of pNP solution with $(PSS/PAH)_3$/ALP deposited on different surfaces (S1−S5); and (b) average catalytic reaction rate, calculated from the slope of the data of panel a, for each surface.

phenyl phosphate (pNP) and fluorescein diphosphate (FDP), respectively. A scheme of the two model catalytic reactions studied is displayed in Figure 6.

The Michaelis−Menten eq 1 has been largely employed to describe the kinetics in enzymatic catalysis for a single enzyme and single substrate. In particular, when the amount of substrate (S), i.e., pNP or FDP, is in excess ($S \gg K_M$), the rate of the catalysis (v_{cat}) can be considered constant and maximum (V_{max}). In our experiments, because the pNP and FDP are present in the solution bulk in a large excess, we can consider the reaction rate constant throughout the whole experiment.

$$v_{cat} = \frac{V_{max} S}{K_M + S} \tag{1}$$

Taking into account these theoretical considerations, the first series of experiments were directed to compare the catalytic activity of the different substrates. For this purpose, the same multilayer system of $(PSS/PAH)_3$/ALP (ALP1) was fabricated on all surfaces. First, the catalysis of pNP was tested. The product obtained in this case is *p*-nitrophenol, a yellow colored compound that was monitored in situ following the absorbance at a wavelength of 405 nm at different times up to 2 h. All surfaces (S1−S5) were placed inside a 6 wells Costar microplate and 2 mL of a solution of pNP (10 mM) in 150 mM NaCl/10 mM Tris buffer (pH 8.0) were added. In parallel, blank experiments were carried out at the same time to avoid any possible signal caused by the natural decomposition of pNP. To correlate the absorbance values obtained with the concentration of *p*-nitrophenol, the Beer−Lambert eq 2 was used with a molar extinction coefficient (ε) of 18 000 M^{-1} cm^{-1}[50] and a light path length (b) of 0.35 cm. Combining the slope (m) obtained by measuring the variation of absorbance with time and the Beer−Lambert equation, the reaction rate can be calculated as depicted in eq 3. Also, because the reaction rate was found to be dependent to the size of the surface employed, we normalized the results to the area of the samples.

$$A = b\varepsilon c \tag{2}$$

$$v_{cat} = \frac{dc}{dt} = \frac{m}{b\varepsilon} \tag{3}$$

In Figure 7a, the evolution of the absorbance as a function of time is shown for different surfaces (S1−S5) functionalized by $(PSS/PAH)_3$/ALP multilayer in contact with pNP solution. It can be seen a strong linear tendency ($R^2 \approx 1$), proving that, as expected, the formation of *p*-nitrophenol is constant with time. The activity of the functionalized surfaces is maintained for, at least, 2 days, without any decrease of the slope indicating a robust catalytic activity of immobilized ALP. In Figure 7b, the reaction rates obtained from the slope of the curves are depicted for each surface. Remarkably, higher catalytic speeds

DOI: 10.1021/acsami.5b02607
ACS Appl. Mater. Interfaces 2015, 7, 12210−12219

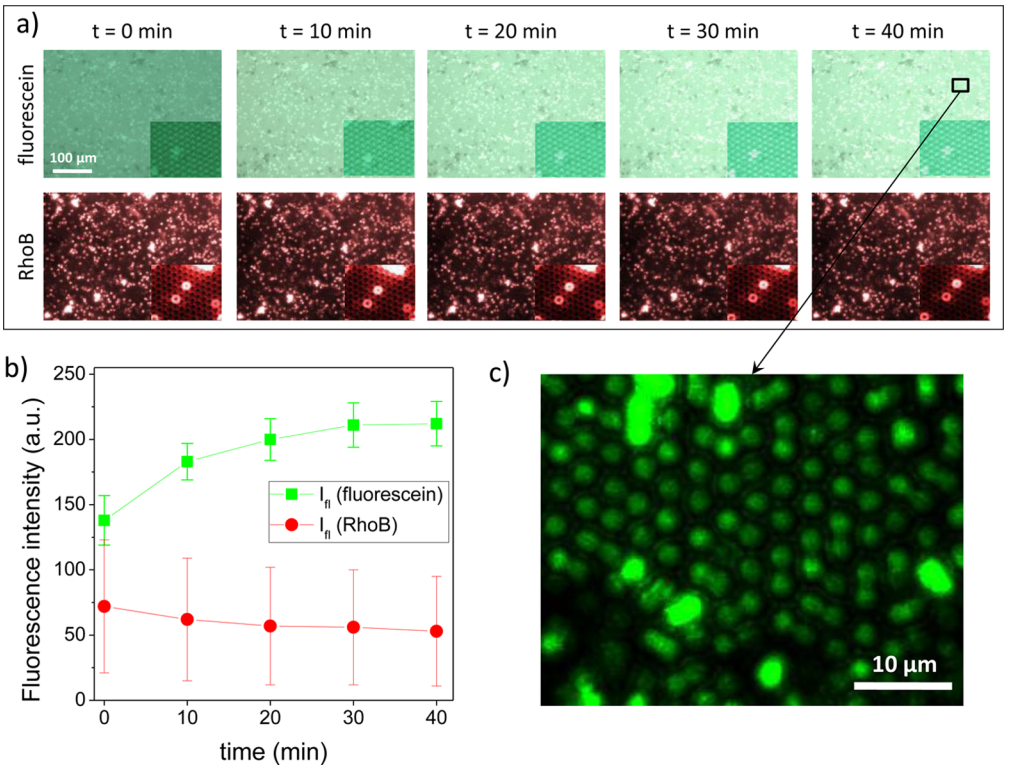

Figure 8. Catalytic activity of immobilized ALP on surface S5; (a) epifluorescence microscopy micrographs of $(PSS/PAH)_3/ALP^{RhoB}$ functionalized surface S5 in contact with a droplet containing 0.1 mg/mL FDP observed at different times (green channel above, red channel below); (b) evolution of the fluorescence intensity, determined from the micrographs, as a function of time for the green channel due to fluorescein (green curve) and the red channel due to ALP^{RhoB} (red curve); (c) magnification of the micrograph, measured on the green channel, obtained after 40 min of contact. The gamma and gain parameters of the image were optimized to completely eliminate the background.

(3 times) are obtained for the porous surfaces (S3, S5) than for all flat ones (S1, S2, S4). Porous surfaces have higher specific surface area due to the presence of pores, which means that more ALP is expected to be available at the surface to participate in the catalytic reaction (see supporting info for more details about specific surface area). This supports the hypothesis we claimed before that the multilayers reach and cover the inner part of the pores. When comparing flat surfaces, the catalytic activity of ALP is slightly higher for surfaces S2 and S4 than for surface S1. ALP seems better adsorbed on polymer blends coated surfaces than on the silicon wafer activated with UVO. Finally by comparing both porous surfaces, the kinetics of the reaction carried out using fluorinated surface S3 is significantly faster than those observed using carboxylated surface S5. It is true that the topography of these two surfaces is not identical (the pore size is somehow different), so they are not perfectly comparable. However, the higher rates obtained using surface S3 cannot be only justified because of the difference in pore size. The distribution of ALP over the entire surface of surface S3 is probably responsible for its higher catalytic activity. On the contrary, in the case of surface S5 due to the specific immobilization of ALP inside the pores, the catalysis only occurs inside them. The possibility to confine chemical reactions within micrometer-sized pores makes these platforms excellent candidates for the design of microreactors.

Further experiments were carried out increasing the number of $(PSS/PAH)_3/ALP$ blocks (ALP2 and ALP3). However, no significant changes on the catalytic activity were observed. Most probably, ALP embedded within the multilayer structure does not play any role during the catalytic reaction. PSS/PAH was previously reported to act as a barrier blocking the access to the inner layers.[51] In view of their potential application to carry out catalytic reactions in confined environments, the enzymatic activity of surface S5, where ALP is localized only inside the holes, was additionally tested. For this purpose, FDP was used as a substrate of ALP to produce fluorescein, monitored in the green channel of the epifluorescence microscope. Besides, the use of ALP^{RhoB} allows localizing the enzyme in the porous surface in the red channel at the same time.

Under an epifluorescence microscope (the surface area analyzed is 0.16 mm^2), a droplet of 0.1 mL of the solution (0.1 mg/mL FDP in 150 mM NaCl) was placed on top of $(PSS/PAH)_3/ALP$ functionalized surface S5. As depicted in Figure 8a, images in both channels were taken immediately upon contact with the solution (t = 0 min) and every 10 min up to 40 min. The average fluorescence intensity measured from each pictures displayed in Figure 8a is plotted in Figure 8b. The fluorescence intensity of the green channel increases gradually and can be associated with the fluorescein released as the product of the catalytic reaction of FDP. However, instead of a linear dependence with time (as observed in the case of pNP), the slope of the curve decreases and may achieve a plateau. This behavior corresponds to a catalytic curve where the substrate is not in excess, so the reaction rate diminishes as the substrate is consumed. Indeed by measuring the absorbance of the supernatant after 40 min, the concentration of the fluorescein released is about 4.7×10^{-5} M (ε = 70 000 $M^{-1}cm^{-1}$), with an initial concentration of FDP (enzymatic substrate) at 1.8×10^{-4} M. Thus, in the experiments done under the microscope, we are not in excess of substrate. More interestingly, when we

DOI: 10.1021/acsami.5b02607
ACS Appl. Mater. Interfaces 2015, 7, 12210−12219

take a closer look to the sample while the reaction is running, the green fluorescence intensity is specifically located inside the holes (Figure 8c). This contributes to the idea that the reaction occurs only inside them, where ALP is localized, proving that these materials can perfectly be used as microreactors. On the red channel, the fluorescence intensity is practically constant, although a slight decrease is observed (Figure 8b). This could be explained by the possible release of ALP^{RhoB} from the surface to the aqueous medium.

CONCLUSIONS

In this publication, we combined the breath figures technique, that allows fabricating porous materials with micrometric pore size and the layer-by-layer technique, which permits to fabricate thin films with controlled thickness and composition. Porous and flat surfaces, with two different functionalities were prepared (carboxylated and fluorinated surfaces) to deposit an enzyme ALP, only inside the pores or all over the surface. A multilayer system of PSS/PAH was first deposited and then a layer of a bioactive compound (i.e., an enzyme, ALP) was immobilized on the different surfaces. The activity of ALP was tested showing that higher catalytic activity is always obtained with porous than with flat surfaces. In the case of fluorinated porous surfaces, the catalytic activity was the highest, around 3 times higher when compared to the flat surface with the same composition. In the case of porous surfaces containing carboxylic acid groups, the localized deposition of multilayers inside the pores allowed obtaining the catalysis specifically inside the holes, where the ALP is located opening potential applications in microreactors systems.

ASSOCIATED CONTENT

Supporting Information

Specific surface area calculus, Figure S1, and Table S1 (PDF). The Supporting Information is available free of charge on the ACS Publications website at DOI: 10.1021/acsami.5b02607.

AUTHOR INFORMATION

Corresponding Authors

*E-mail: alexandra.munnoz@uam.es.

*E-mail: jrodriguez@ictp.csic.es.

Notes

The authors declare no competing financial interest.

ACKNOWLEDGMENTS

This work was financially supported by the MINECO (Projects MAT2010-17016 and MAT2013-47902-C2-1-R (JRH)). A S.d.L. thanks the Ministerio de Educación for his FPU predoctoral fellowship. T.G. thanks FRC for financial support. A.M.-B. gratefully acknowledges the MINECO for her Ramon y Cajal.

REFERENCES

(1) Fadhel, A. Z.; Pollet, P.; Liotta, C. L.; Eckert, C. A. Combining the benefits of homogeneous and heterogeneous catalysis with tunable solvents and nearcritical water. *Molecules* **2010**, *15*, 8400−8424.

(2) Graham, U. M.; Dozier, A.; Khatri, R. A.; Bahome, M. C.; Jewell, L. L.; Mhlanga, S. D.; Coville, N. J.; Davis, B. H. Carbon nanotube docking stations: A new concept in catalysis. *Catal. Lett.* **2009**, *129*, 39−45.

(3) Vriamont, C.; Devillers, M.; Riant, O.; Hermans, S. Catalysis with Gold Complexes Immobilised on Carbon Nanotubes by π-π Stacking Interactions: Heterogeneous Catalysis versus the Boomerang Effect. *Chem.—Eur. J.* **2013**, *19*, 12009−12017.

(4) Chen, P.; Yang, F.; Kostka, A.; Xia, W. Interaction of Cobalt Nanoparticles with Oxygen- and Nitrogen- Functionalized Carbon Nanotubes and Impact on Nitrobenzene Hydrogenation Catalysis. *ACS Catal.* **2014**, *4*, 1478−1486.

(5) MacHado, B. F.; Serp, P. Graphene-based Materials for Catalysis. *Catal. Sci. Technol.* **2012**, *2*, 54−75.

(6) Li, Y.; Shi, J. Hollow-structured Mesoporous Materials: Chemical Synthesis, Functionalization and Applications. *Adv. Mater.* **2014**, *26*, 3176−3205.

(7) Sahiner, N.; Ozay, H.; Ozay, O.; Aktas, N. A Soft Hydrogel Reactor for Cobalt Nanoparticle Preparation and Use in the Reduction of Nitrophenols. *Appl. Catal. B* **2010**, *101*, 137−143.

(8) Colmenares, J. C.; Luque, R. Heterogeneous Photocatalytic Nanomaterials: Prospects and Challenges in Selective Transformations of Biomass-Derived Compounds. *Chem. Soc. Rev.* **2014**, *43*, 765−778.

(9) Ansari, S. A.; Husain, Q. Potential Applications of Enzymes Immobilized on/in Nano Materials: A Review. *Biotechnol. Adv.* **2012**, *30*, 512−523.

(10) Li, Y.; Yan, L.; Liu, Y.; Qian, K.; Liu, B.; Yang, P. High-Efficiency Nano/Micro-Reactors for Protein Analysis. *RSC Adv.* **2015**, *5*, 1331−1342.

(11) Xu, B. B.; Zhang, Y. L.; Wei, S.; Ding, H.; Sun, H. B. On-Chip Catalytic Microreactors for Modern Catalysis Research. *ChemCatChem.* **2013**, *5*, 2091−2099.

(12) Teh, S. Y.; Lin, R.; Hung, L. H.; Lee, A. P. Droplet Microfluidics. *Lab Chip* **2008**, *8*, 198−220.

(13) Ji, J.; Nie, L.; Qiao, L.; Li, Y.; Guo, L.; Liu, B.; Yang, P.; Girault, H. H. Proteolysis in Microfluidic Droplets: An Approach to Interface Protein Separation and Peptide Mass Spectrometry. *Lab Chip* **2012**, *12*, 2625−2629.

(14) Mazutis, L.; Baret, J. C.; Treacy, P.; Skhiri, Y.; Araghi, A. F.; Ryckelynck, M.; Taly, V.; Griffiths, A. D. Multi-Step Microfluidic Droplet Processing: Kinetic Analysis of an in Vitro Translated Enzyme. *Lab Chip* **2009**, *9*, 2902−2908.

(15) Blackledge, C.; Engebretson, D. A.; McDonald, J. D. Nanoscale Site-Selective Catalysis of Surface Assemblies by Palladium-Coated Atomic Force Microscopy Tips: Chemical Lithography Without Electrical Current. *Langmuir* **2000**, *16*, 8317−8323.

(16) Zarzar, L. D.; Swartzentruber, B. S.; Harper, J. C.; Dunphy, D. R.; Brinker, C. J.; Aizenberg, J.; Kaehr, B. Multiphoton Lithography of Nanocrystalline Platinum and Palladium for Site-Specific Catalysis in 3d Microenvironments. *J. Am. Chem. Soc.* **2012**, *134*, 4007−4010.

(17) Meek, C. C.; Pantano, P. Spatial Confinement of Avidin Domains in Microwell Arrays. *Lab Chip* **2001**, *1*, 158−163.

(18) Hoa, M. L. K.; Lu, M.; Zhang, Y. Preparation of Porous Materials with Ordered Hole Structure. *Adv. Colloid Interface Sci.* **2006**, *121*, 9−23.

(19) Muñoz-Bonilla, A.; Fernández-García, M.; Rodríguez-Hernández, J. Towards Hierarchically Ordered Functional Porous Polymeric Surfaces Prepared by the Breath Figures Approach. *Prog. Polym. Sci.* **2014**, *39*, 510−554.

(20) Wan, L.-S.; Zhu, L.-W.; Ou, Y.; Xu, Z.-K. Multiple Interfaces in Self-Assembled Breath Figures. *Chem. Commun.* **2014**, *50*, 4024−4039.

(21) Walter, M. V.; Lundberg, P.; Hult, D.; Hult, A.; Malkoch, M. A One Component Methodology for the Fabrication of Honeycomb Films from Biocompatible Amphiphilic Block Copolymer Hybrids: a Linear-Dendritic-Linear Twist. *Polym. Chem.* **2013**, *4*, 2680−2690.

(22) Ma, H.; Gao, P.; Fan, D.; Du, B.; Hao, J.; Wei, Q. Assembly of Graphene Nanocomposites into Honeycomb-Structured Macroporous Films With Enhanced Hydrophobicity. *New J. Chem.* **2013**, *37*, 1307−1311.

(23) Böker, A.; Lin, Y.; Chiapperini, K.; Horowitz, R.; Thompson, M.; Carreon, V.; Xu, T.; Abetz, C.; Skaff, H.; Dinsmore, A. D.; Emrick, T.; Russell, T. P. Hierarchical Nanoparticle Assemblies Formed by Decorating Breath Figures. *Nat. Mater.* **2004**, *3*, 302−306.

(24) Naboka, O.; Sanz-Velasco, A.; Lundgren, P.; Enoksson, P.; Gatenholm, P. Cobalt (II) Chloride Promoted Formation of

DOI: 10.1021/acsami.5b02607
ACS Appl. Mater. Interfaces 2015, 7, 12210−12219

Honeycomb Patterned Cellulose Acetate Films. *J. Colloid Interface Sci.* **2012**, *367*, 485−493.
(25) Dong, R.; Xu, J.; Yang, Z.; Wei, G.; Zhao, W.; Yan, J.; Fang, Y.; Hao, J. Preparation and Functions of Hybrid Membranes With Rings of Ag Nps Anchored at the Edges of Highly Ordered Honeycomb-Patterned Pores. *Chem.—Eur. J.* **2013**, *19*, 13099−13104.
(26) Pessoni, L.; Lacombe, S.; Billon, L.; Brown, R.; Save, M. Photoactive, Porous Honeycomb Films Prepared from Rose Bengal-Grafted Polystyrene. *Langmuir* **2013**, *29*, 10264−10271.
(27) Siffert, R. S. The Role Of Alkaline Phosphatase in Osteogenesis. *J. Exp. Med.* **1951**, *93*, 415−426.
(28) Wan, L.-S.; Li, Q.-L.; Chen, P.-C.; Xu, Z.-K. Patterned Biocatalytic Films via One-Step Self-Assembly. *Chem. Commun.* **2012**, *48*, 4417−4419.
(29) Deshmukh, P. K.; Ramani, K. P.; Singh, S. S.; Tekade, A. R.; Chatap, V. K.; Patil, G. B.; Bari, S. B. Stimuli-Sensitive Layer-by-Layer (Lbl) Self-Assembly Systems: Targeting and Biosensory Applications. *J. Controlled Release* **2013**, *166*, 294−306.
(30) Decher, G. Fuzzy Nanoassemblies: Toward Layered Polymeric Multicomposites. *Science* **1997**, *277*, 1232−1237.
(31) Lvov, Y.; Antipov, A. A.; Mamedov, A.; Möhwald, H.; Sukhorukov, G. B. Urease Encapsulation in Nanoorganized Microshells. *Nano Lett.* **2001**, *1*, 125−128.
(32) Kamphuis, M. M. J.; Johnston, A. P. R.; Such, G. K.; Dam, H. H.; Evans, R. A.; Scott, A. M.; Nice, E. C.; Heath, J. K.; Caruso, F. Targeting of Cancer Cells Using Click-Functionalized Polymer Capsules. *J. Am. Chem. Soc.* **2010**, *132*, 15881−15883.
(33) Kim, B.-S.; Park, S. W.; Hammond, P. T. Hydrogen-Bonding Layer-by-Layer-Assembled Biodegradable Polymeric Micelles as Drug Delivery Vehicles from Surfaces. *ACS Nano* **2008**, *2*, 386−392.
(34) Yang, W. J.; Pranantyo, D.; Neoh, K. G.; Kang, E. T.; Teo, S. L. M.; Rittschof, D. Layer-by-Layer Click Deposition of Functional Polymer Coatings for Combating Marine Biofouling. *Biomacromolecules* **2012**, *13*, 2769−2780.
(35) Akagi, T.; Fujiwara, T.; Akashi, M. Rapid Fabrication of Polylactide Stereocomplex Using Layer-by-Layer Deposition by Inkjet Printing. *Angew. Chem., Int. Ed.* **2012**, *51*, 5493−5496.
(36) Séon, L.; Parat, A.; Gaudière, F.; Voegel, J. C.; Auzély-Velty, R.; Lorchat, P.; Coche-Guérente, L.; Senger, B.; Schaaf, P.; Jierry, L.; Boulmedais, F. Influence of the Interaction Strength Between Supramolecular Complexes on the Topography of Neutral Polymer Multilayer Films. *Langmuir* **2014**, *30*, 6479−6488.
(37) Yan, Y.; Björnmalm, M.; Caruso, F. Assembly of Layer-by-Layer Particles And Their Interactions With Biological Systems. *Chem. Mater.* **2013**, *26*, 452−460.
(38) Sakr, O. S.; Borchard, G. Encapsulation of Enzymes in Layer-by-Layer (LbL) Structures: Latest Advances and Applications. *Biomacromolecules* **2013**, *14*, 2117−2135.
(39) de León, A. S.; Rodríguez-Hernández, J.; Cortajarena, A. L. Honeycomb Patterned Surfaces Functionalized with Polypeptide Sequences for Recognition and Selective Bacterial Adhesion. *Biomaterials* **2013**, *34*, 1453−1460.
(40) De León, A. S.; Campo, A. D.; Labrugère, C.; Fernández-García, M.; Muñoz-Bonilla, A.; Rodríguez-Hernández, J. Control of the Chemistry Outside the Pores in Honeycomb Patterned Films. *Polym. Chem.* **2013**, *4*, 4024−4032.
(41) Sharpe, J. C.; Mitchell, J. S.; Lin, L.; Sedoglavich, N.; Blaikie, R. J. Gold Nanohole Array Substrates as Immunobiosensors. *Anal. Chem.* **2008**, *80*, 2244−2249.
(42) Mertz, D.; Vogt, C.; Hemmerlé, J.; Mutterer, J.; Ball, V.; Voegel, J. C.; Schaaf, P.; Lavalle, P. Mechanotransductive Surfaces for Reversible Biocatalysis Activation. *Nat. Mater.* **2009**, *8*, 731−735.
(43) Bousquet, A.; Ibarboure, E.; Teran, F. J.; Ruiz, L.; Garay, M. T.; Laza, J. M.; Vilas, J. L.; Papon, E.; Rodríguez-Hernández, J. PH Responsive Surfaces with Nanoscale Topography. *J. Polym. Sci., Part A: Polym. Chem.* **2010**, *48*, 2982−2990.
(44) Haberska, K.; Ruzgas, T. Polymer Multilayer Film Formation Studied By In Situ Ellipsometry And Electrochemistry. *Bioelectrochemistry* **2009**, *76*, 153−161.
(45) Izquierdo, A.; Ono, S. S.; Voegel, J. C.; Schaaf, P.; Decher, G. Dipping Versus Spraying: Exploring the Deposition Conditions for Speeding Up Layer-by-Layer Assembly. *Langmuir* **2005**, *21*, 7558−7567.
(46) Ke, B.-B.; Wan, L.-S.; Li, Y.; Xu, M.-Y.; Xu, Z.-K. Selective Layer-by-Layer Self-Assembly on Patterned Porous Films Modulated by Cassie-Wenzel Transition. *Phys. Chem. Chem. Phys.* **2011**, *13*, 4881−4887.
(47) Mjahed, H.; Porcel, C.; Senger, B.; Chassepot, A.; Netter, P.; Gillet, P.; Decher, G.; Voegel, J. C.; Schaaf, P.; Benkirane-Jessel, N.; Boulmedais, F. Micro-Stratified Architectures Based On Successive Stacking of Alginate Gel Layers and Poly(L-Lysine)-Hyaluronic Acid Multilayer Films Aimed at Tissue Engineering. *Soft Matter* **2008**, *4*, 1422−1429.
(48) Mertz, D.; Vogt, C.; Hemmerlé, J.; Debry, C.; Voegel, J. C.; Schaaf, P.; Lavalle, P. Tailored Design of Mechanically Sensitive Biocatalytic Assemblies Based on Polyelectrolyte Multilayers. *J. Mater. Chem.* **2011**, *21*, 8324−8331.
(49) Zhang, Y.; Wang, C. Micropatterning of Proteins on 3D Porous Polymer Film Fabricated by Using the Breath-Figure Method. *Adv. Mater.* **2007**, *19*, 913−916.
(50) Zhang, Z. Y.; Clemens, J. C.; Schubert, H. L.; Stuckey, J. A.; Fischer, M. W. F.; Hume, D. M.; Saper, M. A.; Dixon, J. E. Expression, Purification, and Physicochemical Characterization of a Recombinant Yersinia Protein Tyrosine Phosphatase. *J. Biol. Chem.* **1992**, *267*, 23759−23766.
(51) Stenzel, M. H. Formation of Regular Honeycomb-Patterned Porous Film by Self-Organization. *Aust. J. Chem.* **2002**, *55*, 239−243.

DOI: 10.1021/acsami.5b02607
ACS Appl. Mater. Interfaces 2015, 7, 12210−12219